Title
Nitrogen-functionalized graphene quantum dot incorporated GelMA microgels as fluorescent 3D-tissue Constructs

Authors
Taravatfard, Aida Zahra
Ceballos-Gonzalez, Carlos
Siddique, Abu Bakar
et al.

Publication Date
2023

DOI
10.1039/d3nr02612

Volume 15
Number 40
28 October 2023
Pages 16231-16502

Nanoscale

rsc.li/nanoscale

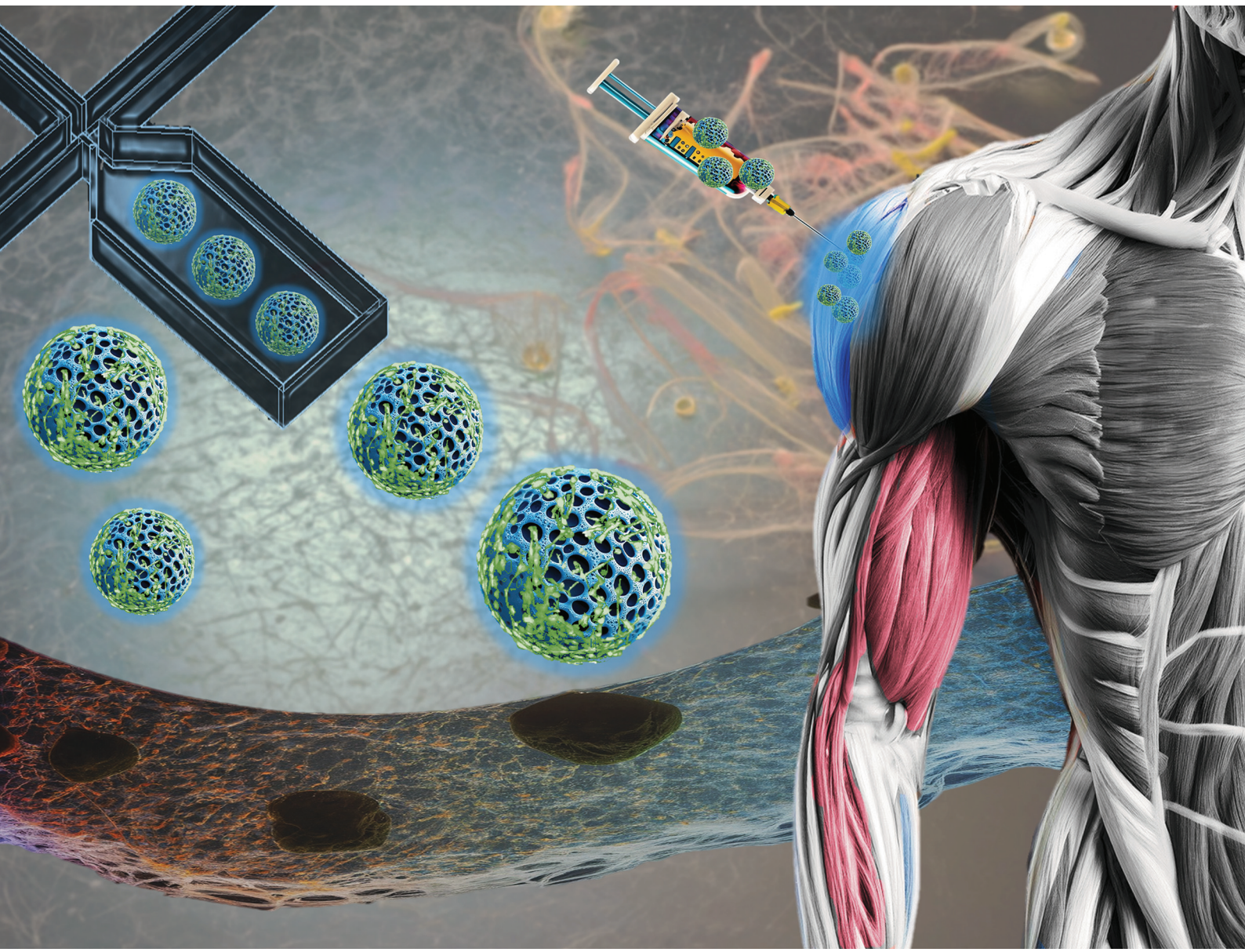

ISSN 2040-3372

ROYAL SOCIETY OF CHEMISTRY

PAPER
Mallar Ray *et al.*
Nitrogen-functionalized graphene quantum dot incorporated GelMA microgels as fluorescent 3D-tissue Constructs

NCNST

Nanoscale

PAPER

View Article Online
View Journal | View Issue

Cite this: *Nanoscale*, 2023, **15**, 16277

Nitrogen-functionalized graphene quantum dot incorporated GelMA microgels as fluorescent 3D-tissue Constructs†

Aida Zahra Taravatfard,‡[a,b] Carlos Ceballos-Gonzalez,‡[a] Abu Bakar Siddique,[a] Johana Bolivar-Monsalve,[a] Masoud Madadelahi,[a] Grissel Trujillo-de Santiago,[c,d] Mario Moisés Alvarez,[c,d] Ashit Kumar Pramanick,[e] Eduardo Martinez Guerra,[f] Lawrence Kulinsky,[b] Marc J. Madou,[a,b] Sergio O. Martinez[a] and Mallar Ray*[a]

Biopolymer microgels present many opportunities in biomedicine and tissue engineering. To understand their *in vivo* behavior in therapeutic interventions, long-term monitoring is critical, which is usually achieved by incorporating fluorescent materials within the hydrogel matrix. Current research is limited due to issues concerning the biocompatibility and instability of the conventional fluorescent species, which also tend to adversely affect the bio-functionality of the hydrogels. Here, we introduce a microfluidic-based approach to generate nitrogen-functionalized graphene quantum dot (NGQD) incorporated gelatin methacryloyl (GelMA) hydrogel microspheres, capable of long-term monitoring while preserving or enhancing the other favorable features of 3D cell encapsulation. A multilayer droplet-based microfluidic device was designed and fabricated to make monodisperse NGQD-loaded GelMA hydrogel microspheres encapsulating skeletal muscle cells (C2C12). Control over the sizes of microspheres could be achieved by tuning the flow rates in the microfluidic device. Skeletal muscle cells encapsulated in these microgels exhibited high cell viability from day 1 (82.9 ± 6.50%) to day 10 (92.1 ± 3.90%). The NGQD-loaded GelMA microgels encapsulating the cells demonstrated higher metabolic activity compared to the GelMA microgels. Presence of sarcomeric α-actin was verified by immunofluorescence staining on day 10. A fluorescence signal was observed from the NGQD-loaded microgels during the entire period of the study. The investigation reveals the advantages of integrating NGQDs in microgels for non-invasive imaging and monitoring of cell-laden microspheres and presents new opportunities for future therapeutic applications.

Received 2nd June 2023,
Accepted 17th August 2023

DOI: 10.1039/d3nr02612d

rsc.li/nanoscale

1 Introduction

Gelatin-methacryloyl, commonly referred to as GelMA, is a photosensitive three-dimensional polymer matrix consisting of gelatin modified by methacrylic anhydride (MA). Due to its favorable properties such as tunable physical characteristics, excellent biocompatibility, biodegradability, and low cost, it is an up-and-coming candidate for 3D cell culture, and tissue engineering.[1,2] Notwithstanding these outstanding properties, cell encapsulation within bulk GelMA and other macro-scale hydrogels suffers from poor nutrient exchange and limited cell–cell communication, causing a lower cell proliferation rate.[3] Microsphere hydrogels, on the other hand, offer a bigger surface-to-volume ratio and a higher similarity to the natural extracellular matrix, which allows for better active nutrient transportation and enhanced cell–matrix and cell–cell interactions, thereby boosting the viability of the encapsulated

[a]*School of Engineering and Sciences, Tecnológico de Monterrey, Monterrey, 64849, Mexico. E-mail: mallar.ray@tec.mx*
[b]*Department of Mechanical and Aerospace Engineering, University of California, Irvine, CA 92697, USA*
[c]*Centro de Biotecnología-FEMSA, Tecnológico de Monterrey, Monterrey 64849, Mexico*
[d]*Departamento de Ingeniería Mecatrónica y Eléctrica, Tecnológico de Monterrey, Monterrey 64849, Mexico*
[e]*National Metallurgical Laboratory, Jamshedpur, 831007 Jharkhand, India*
[f]*Centro de Investigaciones en Materiales Avanzados, CIMAV Unidad Monterrey, Alianza Norte 202, Apodaca, Nuevo León, C.P. 66628, Mexico*

† Electronic supplementary information (ESI) available: Microfluidic device fabrication; generation of hydrogel microspheres: quantum yield measurement; HR-TEM micrographs of NGQDs; additional PL spectra; GelMA-loaded NGQD fluorescence emission; enhancement of structural stability of GelMA microgels following NGQD incorporation. See DOI: https://doi.org/10.1039/d3nr02612d

‡ These authors contributed equally to this work.

cells.[3] Furthermore, during injection, cell-laden microgels protect cells from the imposed shear force and eventually increase the cell survival rate of minimally invasive, *in vivo* treatment.[4] Owing to these features, cell-laden GelMA microgels have been used as injectable hydrogels in therapeutic and cellular delivery applications.[5] Two critical factors for the widespread adoption of cell-laden microsphere technology are the high throughput and monodispersity of the microgels. Recently, droplet-based microfluidic systems have enabled high throughput production of monodispersed microgels with minimal reagent consumption.[6–8]

Despite the above-mentioned remarkable characteristics of cell-laden GelMA microspheres, some serious drawbacks have hampered their real-life and widespread applications. The major challenges include low mechanical stability, low electrical conductivity, and a lack of long-term, non-invasive imaging and monitoring ability of cell-laden microspheres and entrapped cells.[9] So far, many efforts have focused on improving the mechanical and rheological properties of GelMA-based hydrogels for desired applications in specific microenvironments, but the issue of real-time, long-term monitoring and labeling of microgels has received much less attention.[10] Conventionally, organic dyes and fluorescent proteins, including fluorescein,[11] and rhodamine B,[12] are used as tissue and cellular labeling agents in microgels. As a case in point, recent work by Fang *et al.*,[7] integrated microfluidics and bioprinting techniques to develop cell-laden biphasic microgels with excellent rheological properties, but the fluorescence labelling was carried out by fluorescein and rhodamine. The widely used conventional fluorescent molecules are limited due to their organic composition and photobleaching instability.[13] In this regard, light-emitting graphene quantum dots (GQDs) offer an excellent alternative for fluorescent species since they not only render the microgel luminescent for stable and real-time monitoring but also offer the added advantages of enhanced cellular therapy.

Quantum dot (QD)-based labelling has emerged as a promising tool in therapeutic applications.[14] However, the standard semiconductor QDs are known for their toxicity and adverse biological effects.[15] The carbon-based GQDs, unlike the other semiconductor QDs are reported to possess low biological toxicity,[16] improved mechanical and optical tunability,[17] robust photoluminescence (PL),[17] and degradability,[18] while conjugating with different hydrogels. The functionalization of GQDs with nitrogen (NGQDs) enhances charge transfer, storage, surface area, quantum yield, stability, and surface hydrophilicity, all crucial properties for creating a highly fluorescent nanomaterial.[19–21] Furthermore, NGQDs exhibit superior biocompatibility, electrical conductivity, bright fluorescence, and strong resistance to photobleaching, making them promising for the fabrication of fluorescent electro-active scaffolds.[21,22] The improved quantum yield, photoluminescence, and enhanced cellular uptake of NGQDs due to their smaller size, result in a brighter fluorescent signal and make them a promising candidate for long-term studies such as cell–cell interactions and cell differentiation.[23] Several reports have demonstrated the applications of NGQD in cellular biology by 2D cell culturing, and cellular imaging.[24,25] Recently, researchers have shown the reinforcing properties and electrical conductivity enhancement of these nanomaterials in conjugation with different bulk hydrogels, which is favorable for fabricating skeletal muscle tissues.[26] However, the effect of NGQDs on cellular behavior in microgels and 3D microenvironments has not been investigated yet. Skeletal muscle cells serve as an ideal validation model for our platform. In cases of skeletal muscle tissue injury or during the aging process, the regeneration process can become inefficient in elderly individuals or those experiencing muscular atrophy.[27,28] Extracellular matrix-derived microgels offers distinct advantages as cell delivery systems, including a high surface area for cell proliferation, migration, and diffusion of nutrients and oxygen, as well as the ability to be injected into a host tissue.[29,30] These properties make them particularly relevant for muscle tissue engineering. Furthermore, monitoring the engineered tissue after injection is a crucial factor in skeletal muscle engineering.[3,31]

In this work, for the first time, to the best of our knowledge, we have investigated the fabrication of skeletal muscle cell (SMC)-laden fluorescent GelMA microgels, where NGQDs are used as a photo-stable nanomaterial for hydrogel imaging. The NGQD-loaded GelMA microgels were fabricated using a multilayer droplet-based microfluidic system to continuously generate tunable and highly homogeneous microgels. Instead of conventional photolithography in the previous similar studies,[7,32,33] here we have used a simple and inexpensive cutter plotter-based technique to fabricate the microfluidic device that allows the fabrication of cell-laden hydrogels without compromising the size control and shape fidelity. NGQDs have brought excellent myogenic differentiation, cellular proliferation, and viability within the microgels, making this material a promising bioimaging carrier.

2 Experimental

2.1 Materials

Gelatin from Porcine Skin Type A (G2500), methacrylic anhydride (MA), Dulbecco's phosphate buffered saline (DPBS) (D5773), dialysis membrane (D9527-100FT), lithium phenyl-2,4,6-trimethyl-benzoyl phosphinate (LAP), mineral oil (M841), Dulbecco's modified Eagle's medium/high glucose (DMEM; D5648), 4′,6-diamidino-2-phenylindole (DAPI; 3 : 1000, D9542), and Span® 80 were purchased from Sigma-Aldrich. Mouse myoblasts (C2C12; Mus musculus, CRL 1772) were acquired from ATCC®. Dulbecco's modified Eagle medium/high glucose (DMEM; D5648), and 4′,6-diamidino-2-phenylindole (DAPI; 3 : 1000, D9542) were purchased from Sigma-Aldrich (Burlington, MA, USA). Citric acid (100241) was purchased from Merck (India) and ethylenediamine (E479500) was procured from Fisher Chemicals (India). Trypsin-EDTA (25200072), Dulbecco's phosphate-buffered saline (DPBS; 14040141), phosphate-buffered saline (PBS; 10010023), fetal

bovine serum (10437028), and antibiotic/antimycotic (15240062) were purchased from Gibco (Carlsbad, CA, USA). Goat anti-mouse IgM mu chain conjugated with Alexa Fluor 647 (1 : 200; ab150123) was acquired from Abcam (Cambridge, UK). Live/Dead Cell imaging kit (R37601) was purchased from Invitrogen (Waltham, MA, USA). Anti-sarcomeric α-actin (1 : 50; sc-58670) was acquired as a free sample from Santa Cruz Biotechnology Inc. (Dallas, TX, USA).

2.2 Synthesis

2.2.1 GelMA synthesis. Gelatin was dissolved in DPBS at 10% (w/v) and stirred at 300 rpm for one hour at a constant temperature of 50 °C. Subsequently, 10% (v/v) of MA was added into the gelatin solution at the rate of 0.5 mL min^{-1} using a syringe pump. The reaction was allowed to continue for 2.5 hours at a constant temperature (55 °C) and stirring conditions. The reaction was terminated by adding a 5× volume of DPBS. To remove salts and methacrylic acid (a reaction byproduct), the mixture was continuously dialyzed against distilled water by filtering through a 12–14 kDa cutoff dialysis membrane for one week at 37 °C and using a peristaltic pump (Masterflex), at the flow of 5 mL min^{-1}. Finally, the solution was lyophilized in a vacuum freeze dryer for five days to generate a porous white foam that was stored at −80 °C before use.

2.2.2 NGQD synthesis. Colloidal suspensions of NGQDs were synthesized by the hydrothermal treatment of a mixture of 2.1 g of citric acid and 1.8 g ethylene diamine in 50 mL DI water in an autoclave following Qu *et al.*[20] A sealed Teflon-lined stainless-steel autoclave was heated to 180 °C in an oil bath and kept for additional 8 hours. Finally, colloidal NGQDs were collected and stored in the refrigerator after centrifugation at 5000 rpm for 10 min.

2.2.3 GelMA-NGQD preparation. To generate prepolymer GelMA-NGQD, lyophilized GelMA was mixed at 5% (w/v) into DPBS containing 0.015% (w/v) NGQD and 0.2% (w/v) of lithium phenyl-2,4,6-trimethylbenzoylphosphinate (LAP) in low lighting conditions. Complete dissolution was achieved by placing the reaction tube in a 70 °C water bath for 20 minutes. Finally, the solution was stored in a −4 °C refrigerator for further use.

2.3 Multilayer droplet based-microfluidic chip fabrication

The multilayer droplet-based microfluid platform was made by the alignment of seven plastic layers (Fig. S1, ESI†). To make channels with varying heights along the flow direction, different types of plastic sheets with different designs were used for the chip alignment, including polyvinyl chloride (PVC, thickness: 0.1 mm), pressure-sensitive adhesive (PSA, thickness: 0.07 mm), and acrylic (thickness: 2 mm). Most of these materials are extremely low-cost and widely accessible. A laser cutter was used to cut the inlets and outlet on the acrylic layer (Glowforge laser printer), and a cutter plotter (Graphtec CE7000-40) was utilized to cut the design on the PSA and PVC layers. The inlets and outlets of the chip were laser cut on an acrylic sheet.

2.4 Microgel generation and size adjustability

The multilayer droplet-based microfluidic setup for GelMA-NGQD microgels fabrication consisted of the following: (i) the fabricated microfluidic chip connected to two syringe pumps, (ii) a UV source (OmniCure S2000) for crosslinking, and (iii) a microscope for size measurement. To generate GelMA-NGQD microgels, the following solutions were injected by syringe pumps; (1) a NGQD-GelMA (5% w/v) solution with 0.2% LAP was injected into the core-flow inlet, and (2) mineral oil enriched with 2% span® 80 solution was injected into the continuous-flow inlet. Once the droplets were generated, they underwent primary UV crosslinking. A low-power UV flashlight was used on the downstream long channel to induce partial photo-crosslinking of microgels (Fig. S2, ESI†). Then, the microgels were collected from the microfluidic chip outlet into multi-well plates and the excess oil was removed by careful pipetting and multiple washing with PBS. Finally, the collected microgels were exposed to a high-power UV laser for 20s for further crosslinking. The size of the generated microgels was controlled by varying the flow rate of the GelMA-NGQD stream while keeping the flow rate of mineral oil constant. A Zeiss Axio Observer Z1 microscope (Zeiss, Germany) equipped with Colibri.2 LED illumination and an Apotome.2 system (Zeiss) was used for the visualization of the microgels. Image analysis was conducted using ImageJ software by Fiji.

2.5 Characterization

2.5.1 Structural characterization. High resolution transmission electron microscopy (HR-TEM) imaging of the NGQDs was done with a JEOL-JEM 2010 operating at 200 kV. Electron energy loss spectroscopy (EELS) analysis was carried out with the GATAN energy filtered TEM integrated with JEM 2010. X-ray photoelectron spectroscopy (XPS) was carried out using Thermo Fisher ESCALAB 250Xi with Al Kα (1486.6 eV) radiation source. Fourier transform infrared (FTIR) and UV-visible spectra were collected by a JACSO 4700 LE and a JASCO V-750, respectively. Zeta potential of NGQDs with concentration of 0.015% (w/v) was measured using Zetasizer (Malvern, UK).

2.5.2 PL and PL quantum yield measurement. The PL spectra of the NGQDs, GelMA, GelMA-NGQD samples were recorded using Cary Eclipse fluorescence spectrometer at NGQDs concentration of 0.015% (w/v). For PL measurement, samples were excited within the range of 350 nm to 450 nm and an integration time of 0.5 s and fixed slit width of 1 nm was maintained for all measurements. For the PL quantum yield, the integration window of the emission spectra was fixed between 380 nm to 700 nm. The PL quantum yield of NGQD and NGQD-GelMA colloids were measured using rhodamine 6G as the reference (for details of PL quantum yield determination, please see ESI, section S3†).

2.5.3 Rheological characterization. Rheological investigations were performed utilizing a TA Instruments Discovery Hybrid Rheometer-2, where measurements of viscosity and frequency sweep were carried out *via* implementation of a 20 mm and 12 mm parallel plate equipped with a Peltier plate steel.

To assess the viscosity of GelMA and GelMA-NGQD hydrogels, 300 μL of the solutions were pipetted onto a plate. To conduct frequency sweep measurements, samples of pill-shaped geometry were fabricated by introducing 100 μL of GelMA and GelMA-NGQD solutions into a 96 well-plate, which prepared as outlined in section 2.3. Following this, the samples were cross-linked by exposure to a UV source for a duration of 60 seconds. The effect of shear rate on the viscosity of GelMA and GelMA-NGQD samples were investigated by a rheology test under shear rate range of 0.1 to 100 s^{-1}. Frequency sweep measurements were performed for UV-cured samples by setting parameters at 102.2 mm gap, 1% strain, and an angular frequency range of 0.1 to 10 rad s^{-1}. All experiments were performed at 25 °C.

2.6 Cell culture and flexible encapsulation of cells

Mouse myoblasts (C2C12 cell line, ATCC) were cultured in DMEM medium supplemented with 10% fetal bovine serum (FBS, Gibco) in 75 mL T-flasks at 37 °C in a humidified atmosphere of 5% CO2. For the encapsulation experiments, cells were detached from the culture surfaces using 0.25% trypsin-ethylene diamine tetra acetic acid (EDTA) and resuspended in GelMA 5% (w/v). These suspensions were prepared at a final cell density of 5×10^6 C2C12 cells per mL. The cell suspension was injected into the inner channel of the microfluidic chip.

2.7 Cell viability

Microgels were washed using PBS and covered with Live/Dead® reagent on days 1, 5, and 10. After incubation at 37 °C for 30 min, microgels were washed three times with PBS and imaged using a 10× objective in an Axio Observer Z1 microscope equipped with a Colibri.2 LED illumination and an Apotome.2 system (Zeiss, Jena, TH, Germany). A LED intensity of 60% and an exposure time of 400 ms were established for FITC channel. Similarly, a LED intensity and exposure time of 90% and 1000 ms, respectively, were settled for the EtHD1 channel. Cell viability was calculated as the ratio between the covered area for viable (green) cells and the total cell area. Five images per day were analyzed using Fiji® software.

2.8 Metabolic activity

The metabolic activity of cells encapsulated in microgels with, or without NGQDs was assessed by the PrestoBlue® assay, as described by Bolívar-Monsalve *et al.*[34] For this purpose, approximately 30–40 constructs per well were cultured in non-adherent 24-well plates. At specific time points (0, 1, 5, and 10 days), the microgels were incubated with DMEM/high glucose containing 10% PrestoBlue® reagent (Invitrogen) at 37 °C for 1 h. The fluorescence intensity of the PrestoBlue® solution was measured at 530/570 nm excitation and emission wavelengths, respectively, using a microplate reader (Synergy HTX Multi-mode, BioTek, USA). The background signal was subtracted using a blank, and readings were normalized with respect to day 0. At least three samples from four biological replicates were used for calculations.

2.9 Sample embedding and immunostaining of muscle cells

Microgels on day 10 were embedded in a PBS solution containing 7% (w/v) gelatin and 10% (w/v) sucrose as previously described by Bolívar-Monsalve *et al.*[34] Immunostaining of C2C12 cells were carried out based on the protocol reported previously.[34] Briefly, a 4% (v/v) paraformaldehyde solution was added to the embedded microgels for 20 min at 25 °C for cell fixation. The cell membrane was permeabilized using Triton X-100 (0.5% v/v) for 45 min at 25 °C and rinsed three times with PBS. Then, samples were blocked using 0.3 M glycine, Triton X-100 (0.5% v/v), and bovine serum albumin (5% w/v) in PBS solution followed by overnight incubation at 4 °C. The blocking solution was removed, and a solution containing the anti-sarcomeric α-actin (1 : 50) primary antibody in the blocking solution was added and incubated overnight at 4 °C. The samples were washed using PBS and incubated overnight with an Alexa Fluor 647 (1 : 200) secondary antibody at 4 °C. Finally, the samples were washed and counterstained using DAPI (3 : 1000) in PBS. 3D reconstructions were integrated using an Axio Observer Z1 microscope equipped with a Colibri.2 LED illumination and an Apotome.2 system (Zeiss).

2.10 Statistics

To evaluate the significant difference between samples, (ANOVA) followed by the Games-Howell *post hoc* test was performed with the mean difference significant at the $p < 0.05$. Multiple means were compared. Group comparisons were conducted using Student's *t*-test. The statistical significance was defined as $*p < 0.05$ and $***p < 0.001$. In the biological experiment, at least two biological replicates by triplicate were analyzed. Error bars were defined by standard deviations. Statistical analysis was performed using SPSS software.

3 Results and discussion

3.1 Structural features of NGQDs

The overall structural and surface features of the hydrothermally synthesized NGQDs are summarized in Fig. 1. The bright field HR-TEM image of the NGQDs (Fig. 1a) reveals small crystalline islands corresponding to the graphene dots. The sizes of these nearly spherical dots vary from ~1–5 nm with a modal size of 2.75 ± 0.4 nm. The size distribution (inset, Fig. 1a) was constructed from several similar TEM micrographs (Fig. S4, ESI†). The crystalline character of the dots becomes evident from the high magnification image and the selected area electron diffraction pattern (SAEDP), shown in Fig. 1b and c, respectively. Typical (002) exposed graphitic planes are indicated in Fig. 1b. Further insight into the structure of NGQDs is obtained from the EELS data presented in Fig. 1d. The low-loss EELS spectrum shows peaks at 5.5 eV and 14.2 eV due to the π^* surface plasmon and $\pi^* + \sigma^*$ bulk plasmon, respectively. The positions of these peaks indicate the formation of graphene layers. The appearance of $\pi^* + \sigma^*$ bulk plasmon peak at 14.2 eV is suggestive of the formation of graphene monolayers.[35] The introduction of nitrogen in the graphene layer is manifested by the

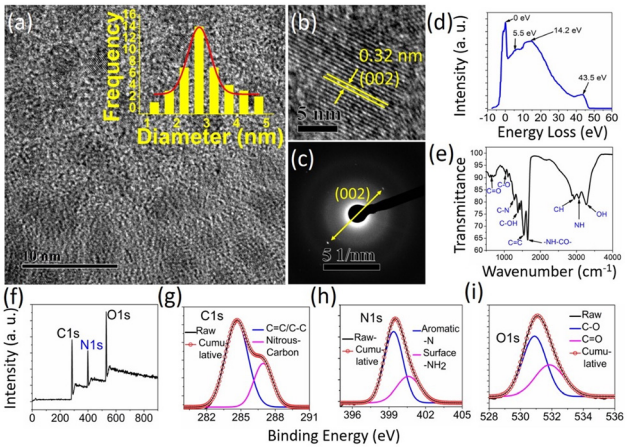

Fig. 1 Structural features of the synthesized NGQDs: (a) Bright field HR-TEM image, inset: the size distribution histogram; (b) high magnification image revealing the (002) planes; (c) SAEDP corresponding to the image in (a); (d) EELS profile of the NGQDs; (e) FTIR spectrum of the NGQDs; (f) XPS wide scan spectrum; deconvoluted (g) C1s; (h) N1s and (i) O1s, high resolution XPS spectra.

hump peaking at 43.5 eV.[36] The FTIR spectrum of NGQDs, shown in Fig. 1e, further consolidates the formation of a nitrogen-functionalized structure. The band peaking at 3270 and 3075 cm^{-1} is due to in-plane stretching vibrations of O–H and N–H, respectively.[37] The peaks at 1650 cm^{-1} and 1272 cm^{-1} correspond to the stretching vibrations of –NH–CO and C–N respectively, indicating the incorporation of nitrogen atoms into the graphitic nanostructure.[38] In addition to that, some other peaks identified at 1540 cm^{-1}, 1380 cm^{-1}, 1037 cm^{-1} and 660 cm^{-1} corresponds to the vibrations of C=C, C–OH, C–O and C=O, respectively.[39]

XPS measurements were performed to understand the surface chemical structure of the synthesized NGQDs. Three strong peaks were detected in the wide-scan XPS spectrum of NGQDs at 285 eV, 400 eV, and 530 eV that correspond to oxygen, nitrogen, and carbon, respectively, as shown in Fig. 1f.[20] The high-resolution C1s XPS spectrum (Fig. 1g) deconvolutes into two components, corresponding to C=C/C–C (sp^2/sp^3 carbon) and nitrous-carbon at 284.6 eV and 287 eV, respectively.[40] The de-convoluted N 1s spectra shown in Fig. 1h, confirms the presence of aromatic-N and surface-NH_2 corresponding to the two components at 399.25 and 400.25 eV.[41] The O1s spectrum (Fig. 1i) can be de-convoluted into two components, peaking at 531.1 eV due to the C–O and 532.2 eV due to C=O groups.[42] The presence of surface-NH_2 in the high-resolution N1s de-convoluted peak ensures surface passivation by amines in the NGQDs, which is also confirmed by the presence of N–H bonding vibration observed in the FTIR spectrum. Therefore, the results of HR-TEM, EELS, FTIR, and XPS confirm the formation of NGQDs.

3.2 NGQD incorporated GelMA microgel

GelMA hydrogel microspheres containing 0.015% (w/v) of NGQDs were prepared by a specially designed multilayer droplet-based microfluidic device that was fabricated by a simple and inexpensive cutter plotter-based technique. Details of device fabrication and microgel generation are discussed in the experimental section and in the ESI.† GelMA-NGQD hydrogel with GelMA concentration of 5% (w/v) was used in this study. Dynamic light scattering indicated a zeta potential of −17 mV for NGQDs, which facilitates their physical interaction with positively charged gelatin and the formation of GelMA-NGQD composite system. To assess the effect of NGQD incorporation on the microgels, GelMA microspheres with and without NGQDs were fabricated (Fig. 2a and b, respectively). The results show that there is a negligible difference between the average size of the generated GelMA microgels (111.18 ± 2.62 μm) and the NGQD incorporated microgels (110.23 ± 5.42 μm). The shape fidelity is also preserved. Importantly, the size of the NGQD-loaded GelMA microgels can be fully controlled by modifying the oil and GelMA-NGQD flow rates. Here, we demonstrate the size adjustability of NGQD-loaded GelMA microgels by controlling the GelMA-NGQD flow rate and fixing the oil flow rate at 3.6 mL h^{-1}. Fig. 2c shows the direct effect of GelMA-NGQD flow rate on the overall size of the microgels. As the flow varies from 0.01 to 0.28 mL h^{-1}, the microgel diameter increases significantly from 142.06 ± 3.56 μm to 503.41 ± 11.66 μm (***$p < 0.001$). Microgels with the smallest (142.06 ± 3.56 μm) and largest (503.41 ± 11.66 μm) sizes are shown in Fig. 2d and e, which were generated at GelMA flow rates of 0.01 and 0.2 mL h^{-1}, respectively. Fig. 2f shows the particle size distribution of the NGQD-loaded GelMA microspheres having an average diameter of 146.43 ± 8.10 μm, which were generated for flow rates of 0.02 and 3.60 mL h^{-1} for GelMA-NGQD and oil solutions, respectively. The coefficient of variation (CV) is calculated to be

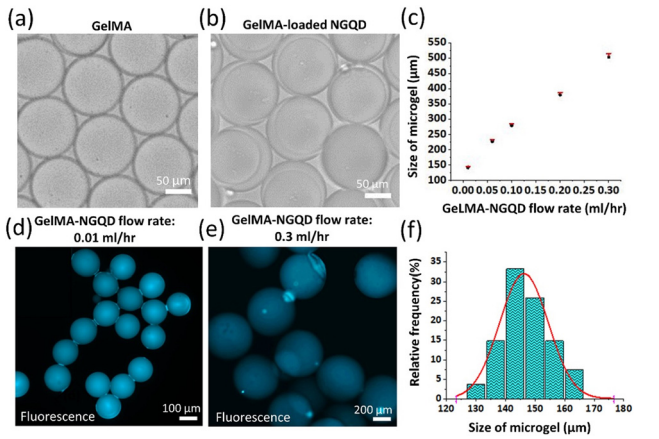

Fig. 2 Size control of NGQD incorporated GelMA microgels. (a) Bare GelMA microgels, (b) NGQD-loaded GelMA microgels (c) variation of the microgel diameter as a function of the GelMA-NGQD flow rates (oil flow rate was maintained at 3.6 mL h^{-1}). The concentration of GelMA was fixed at 5% (w/v). Fluorescence images of the NGQD-loaded GelMA microspheres with wide variation in diameters, (d) smallest spheres with average diameter 142.06 ± 3.56 μm, and (e) largest microspheres having average diameter 503.41 ± 11.66 μm; (f) size distribution of the NGQD-loaded GelMA microgels having an average diameter of 146.43 ± 8.10 μm (***$p < 0.001$).

5.55%. This CV is comparable with the reported microgel sizes generated by microfluidic devices fabricated by double photolithography.[32]

The incorporation of NGQDs makes the hydrogels luminescent under external excitation. The bright room-temperature luminescence is clearly discernible with the naked eye, as shown in Fig. 3a. Although not evident from simple visual inspection, GelMA itself is very weakly luminescent under UV excitation, with a PL emission peak around 450 nm for 350 nm excitation (Fig. 3a and ESI, Fig. S5a†).[43] The NGQDs, on the other hand, are well known to exhibit intense room temperature luminescence,[44] and typically, the PL emission from NGQDs can be tuned by varying the excitation energy.[45] The PL spectra of the NGQD samples prepared and used in this study were collected for excitations varying between 350 and 450 nm and are shown in Fig. 3b. Following the incorporation of the NGQDs in GelMA, the overall features of the spectra remain nearly the same as is evident from Fig. 3b and c. Both for bare NGQD (Fig. 3b) and NGQD incorporated GelMA (Fig. 3c), the PL emission peaks shift from ~450 to 550 nm as the excitation varies from 350 to 450 nm. GelMA affects a nominal quenching of PL (Fig. S5b, ESI†). The relative quantum yield of NGQD and GelMA-NGQD samples, with respect to rhodamine 6G, were calculated to be 77% and 68%, respectively (ESI, Fig. S3†). The high quantum yield of NGQD is in accordance with the previous reports.[19,20] The preservation of the PL features of NGQDs following incorporation in the GelMA matrix and its high quantum yield suggests that that the photophysical characteristics of NGQD remain more or less intact after incorporation in the GelMA matrix, which is essential for imaging application.

One of the major attributes that a bio-functional hydrogel must possess is suitable rheological properties that enable injectability and 3D printing capabilities. Hydrogels with lower storage modulus, higher loss modulus and shear-thinning behaviour are more promising as injectable biomaterials. It is well known that GelMA microgels exhibit shear thinning behaviour and low storage modulus.[46] Here, we investigated the effect on these parameters following the addition of NGQDs. From Fig. 4a, we see that incorporation of NGQDs at

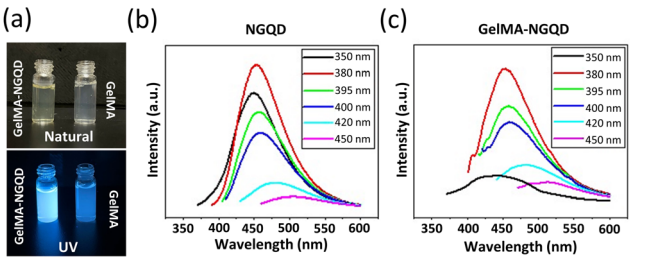

Fig. 3 PL characteristics of bare NGQD and GelMA-NGQD. (a) Optical images of GelMA and GelMA-NGQD hydrogel under natural light (top), and under 385 nm excitation (bottom). PL emission under varying excitation of (b) NGQD, and (c) GelMA-NGQD. The concentration of NGQD was set at 0.015% (w/v).

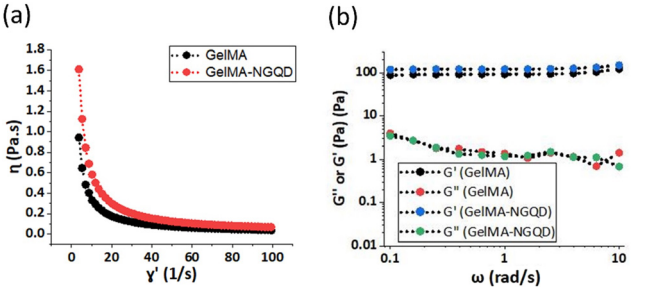

Fig. 4 Rheological properties of GelMA and NGQD incorporated GelMA. Plots of (a) viscosity *versus* shear rate demonstrating shear thinning behaviour of GelMA and GelMA-NGQD gels, (b) frequency sweep for GelMA and GelMA-NGQD hydrogels, using the described method and rheological parameters.

the concentration level used in this work, does not affect the shear-thinning behaviour of GelMA hydrogel. The flow curves of viscosity (η), against strain rate (γ) of polymerized GelMA and GelMA-NGQD samples are very similar. In both cases the viscosity decreases almost identically as the shear rate increases, indicating shear-thinning behaviour. Fig. 4b demonstrates the variation of storage modulus (G') and loss modulus (G'') with the angular frequency (ω). We see that GelMA-NGQD hydrogel exhibits marginally higher storage modulus than GelMA hydrogel; the storage modulus of GelMA-NGQD and GelMA are ~150 Pa and 122 Pa, respectively. Moreover, for both samples G' is higher than G'' throughout the frequency domain, indicating that the materials are essentially elastic.[47] In short, the gross rheological features of the GelMA-NGQD hydrogel are indicative of its suitability for injectability processes and bioprinting.

3.3 Encapsulation of mammalian cells

To the best of our knowledge, all previous studies exploring the biological applications of NGQDs have been performed using 2D-cell culture techniques, wherein NGQDs were added directly to the culture medium.[25,48] Here, we have used the GelMA microgel as a 3D-culture platform to encapsulate both NGQDs and skeletal muscle cells. The cytocompatibility of NGQDs was assessed using C2C12 cells embedded in 5% (w/v) GelMA-based microgels containing 0.015% (w/v) NGQDs (Fig. 5a). This hydrogel composition allowed C2C12 cells to elongate in the microgel on day 5 as shown in Fig. 5b-I. The orthogonal projection shows the presence of cells at the bottom and middle of the scaffold. The NGQD-loaded microgels exhibited fluorescence signals during the entire culture period (Fig. 5b-II, ESI, Fig. S6†). This indicates the durability of NGQD properties after exposure to UV light and over time. Cell viability was assessed by the Live/Dead® assay on days 1, 5, and 10 (Fig. 5c). Cell-laden microgels without NGQDs were used as a control treatment. Cell viability was found to be 82.9 ± 6.5% for the NGQD-loaded microgels and 69.9 ± 11.2% in the control on day 1 (Fig. 5d-I). After five days, cells encapsulated in the presence of NGQDs exhibited a significantly

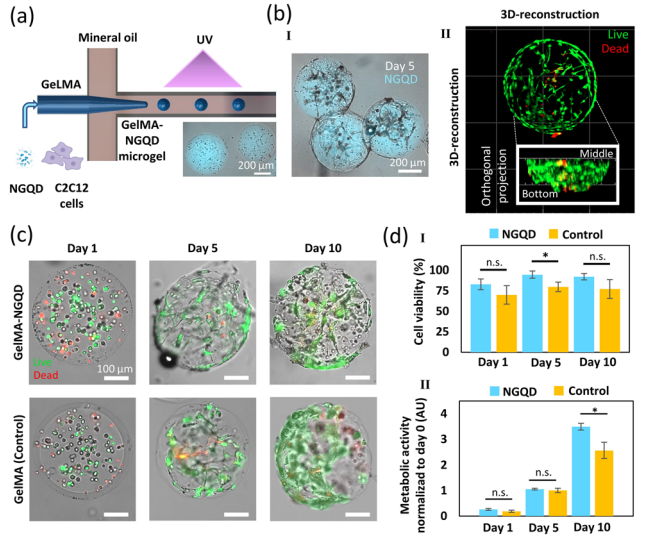

Fig. 5 Cell viability of C2C12 cells encapsulated in microgels containing NGQDs. (a) Schematic representation of the fabrication of cell-laden NGQD-loaded GelMA microgels. (b) (I) Morphological assessment of a microgel showing elongated cells on day 5. Cells were stained with a Live/Dead viability kit. (II) Cell-laden microgels showing the presence of NGQDs (blue) after 10 days of cultivation. (c) Live/Dead staining of constructs on days 1, 5, and 10. (d) (I) Cell viability results on day 1, day 5 and day 10, assessed by image analysis after Live/Dead staining. (II) Metabolic activity of cell-laden microgels measured by PrestoBlue assay. $n = 4$ for each time point. *p-value < 0.05.

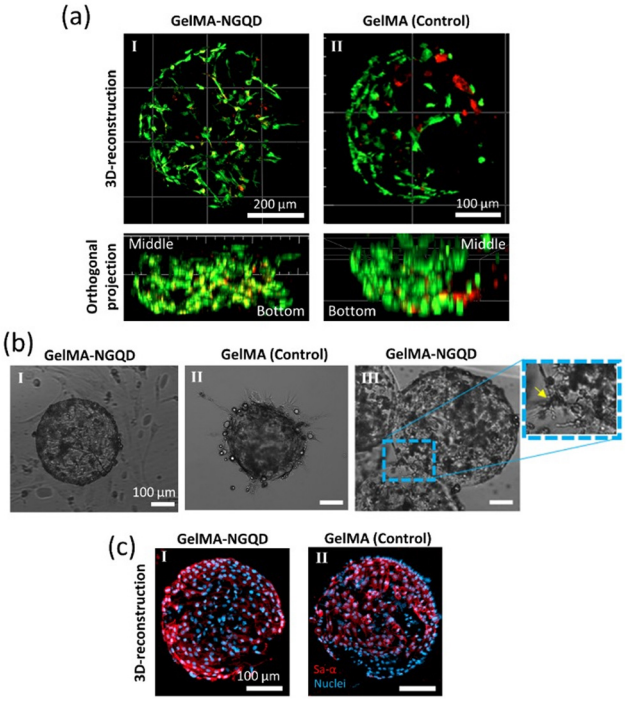

Fig. 6 Elongation, cell migration and immunostaining of C2C12 cells encapsulated in GelMA and GelMA-loaded NGQD microgels on day 10. (a) Z-stacked images of cell-laden microgels in the presence (I) or absence (II) of NGQDs. The orthogonal projections show that C2C12 cells were able to elongate at different Z-planes, suggesting that the microgel composition was cell-friendly. (b) Cell migration in (I) GelMA microgels and (II) NGQD-loaded GelMA on day 10 and (III) the interaction between cells within adjacent microgels. (c) Immunostaining against sarcomeric α-actin in microgels with (I) or without (II) NGQDs.

higher viability (94.5 ± 4.2%) than their counterparts encapsulated without the NGQDs (79.7 ± 5.8%). Cell viability remained high on day 10 for both samples. This confirms that NGQD, at the concentration used, does not exhibit cytotoxic effects on cells (Fig. 5d-I). The increase in cell viability over time in both control and NGQD-loaded GelMA microgels suggests cell proliferation.[6]

The metabolic activity of C2C12 cells, assessed by the PrestoBlue® assay, increased significantly during the cultivation period (Fig. 5d-II). Non-significant differences were found in presence (0.26 ± 0.04 A.U.) or absence (0.19 ± 0.04 A.U.) of NGQDs on day 1. A similar trend was observed on day 5. After 10 days, the metabolic activity was significantly higher in presence of NGQDs (3.49 ± 0.13 A.U.) than in microgels without NGQDs (2.57 ± 0.31 A.U.) (Fig. 5d-II). These results suggest that microgels loaded with 0.015% NGQDs enhance the metabolic activity of C2C12 cells in a time-dependent manner.

Moreover, viable and elongated cells were observed in the inner and outer regions of the microgels on day 10 (Fig. 6a). A higher number of viable cells was observed on the microgel surface than in its middle region. This could be due to nutrient transport limitations to the inner section of the microgels. In addition to cell viability, the ability to migrate is also a vital factor for determining the biocompatibility of the NGQD-loaded GelMA microgels for tissue engineering applications.[49] Fig. 6a shows cell migration from the interior of microgels to the outer environment for both the control and the NGQD incorporated GelMA samples. The interactions between encapsulated cells of neighbouring microgels are beneficial for graft and host interaction (Fig. 6b).

The effect of NGQDs on cell viability has been investigated in the context of cancer therapy. Reports suggest that the maximum cytocompatible concentration of NGQDs is between 0.01 and 0.02% (w/v) for ovarian and breast cancer cells.[25,50] However, studies identifying safe concentrations of NGQDs in healthy cells are scarce. For example, rat bone mesenchymal stem cells can undergo osteogenic differentiation at a concentration of NGQDs lower than 0.01% (w/v).[51] Murine macrophages exhibit ~80% cell viability at NGQD concentrations ranging from 0.01 to 0.02% (w/v).[48] In our study, the concentration of NGQDs in the microgel formulation (0.015% w/v NGQDs) was kept within the range mentioned before (0.01–0.02% w/v). Cell viability results on day 1 suggest that NGQDs at 0.015% (w/v) were not harmful for C2C12 myoblasts compared to the control treatment (*i.e.*, microgels without NGQDs). These results are in accordance with reports performed using healthy,[48] and cancer cells at similar concentrations of NGQDs.[25,50] In addition, cell viability results obtained in this study are within the range reported by others for C2C12 cells (~80–95% viability) encapsulated in pristine GelMA-based microgels,[7] and other GelMA-based constructs.[28,34,52]

Next, the myogenic differentiation of C2C12 cells was assessed by immunostaining against sarcomeric α-actin on day 10. This protein is expressed in skeletal muscle cells during the emergence of myotubes, *i.e.*, the functional cell unit in the skeletal muscle tissue.[28,34] As seen in Fig. 6c, sarcomeric α-actin was found in the presence or absence of NGQDs. Therefore, NGQDs at a concentration of 0.015% do not inhibit the myogenic differentiation of C2C12 cells in GelMA-based microgels. A previous report suggested that 0.018% carbon quantum dots allow differentiation of C2C12 cells cultivated in monolayer (2D-culture) in the presence of a myogenic differentiation medium.[53] In this study, the use of differentiation medium was not required for the expression of sarcomeric α-actin in GelMA-based microgels loaded with C2C12 cells and NGQDs (Fig. 6c). The high surface area per volume in microgels probably facilitated myogenic differentiation,[31] by enhancing the diffusion of nutrients and oxygen.[31] An enhanced access to oxygen and nutrients contributes to the myogenic differentiation of C2C12 cells embedded in hydrogel constructs.[34] Scaffolds with a high surface area also facilitate cell–cell contact and the assembly of skeletal muscle cells to produce consolidated muscle-like tissues.[54] The occurrence of myogenic differentiation in GelMA-based microgels has been reported after 10–14 days of cultivation,[7,55] as also shown in the present study. However, to our knowledge, this is the first investigation that demonstrates the culture of C2C12 myoblasts in the presence of NGQDs. Our results suggest that the use of a concentration of 0.015% (w/v) NGQDs results in high cell viability (~80–95%) and does not inhibit the myogenic differentiation of C2C12 myoblasts encapsulated in 5% (w/v) GelMA microgels. The incorporation of NGQDs in microgel formulations enabled the fabrication of GelMA-based microgels suitable for the emission of a lasting fluorescence signal. Labelling of gelatin using GQDs has been previously proposed as a strategy for long-term tracking after subcutaneous implantation.[13] Future studies should assess the suitability of NGQD as additives for monitoring microgel fate during therapeutic interventions.

4 Conclusions

In summary, we fabricated skeletal muscle cell-laden GelMA microgels incorporating light emitting NGQDs, using a multilayer droplet-based microfluidic system. Fluorescent NGQDs were first synthesized hydrothermally and characterized to ensure the formation of quasi-0D, nitrogen functionalized 2D graphitic structures.

A multilayer droplet-based microfluidic device was designed and fabricated using an inexpensive cutter plotter-based technique and was utilized to prepare monodisperse spherical microgels loaded with the light emitting NGQDs. The sizes of the hydrogel microspheres could be easily controlled and varied by modifying flow rates. The overall luminescent characteristics of the NGQDs were found to remain nearly unaltered following incorporation in GelMA. The rheological measurements revealed that the GelMA-NGQD hydrogels exhibit shear thinning behaviour and marginal enhancement in storage modulus. This confirms the injectability of this hydrogel. GelMA microgels with and without NGQDs were tested for cytotoxicity against the C2C12 cell line. The loaded microgels with a 0.015% (w/v) concentration of NGQDs exhibited higher viability (94.5 ± 4.2%) and higher metabolic activity (3.49 ± 0.13 A.U.) than control samples by day 10. Cell migration and proliferation were also observed in the GelMA-loaded NGQD microgels, revealing the biocompatibility of NGQD in 3D scaffolds. Immunostaining experiments suggest that NGQD-loaded GelMA microgels do not inhibit the myogenic differentiation of encapsulated C2C12. This study demonstrates the potential of NGQDs as an effective additive to injectable cell-laden microgels for *in vivo* and long-lasting monitoring and is a step forward in the aim of fabricating fluorescence-emitting engineered microtissues.

Author contributions

The manuscript was written through contributions of all authors. All authors have given approval to the final version of the manuscript.

Conflicts of interest

The authors declare no competing interest.

Acknowledgements

EJBM and CFCG gratefully acknowledge financial support granted by CONAHCyT (Consejo Nacional de Humanidades, Ciencias y Tecnologías, México) in the form of Graduate Program Scholarships. GTdS acknowledges funding received from CONAHCyT and L'Oréal-UNESCO-CONACyT-AMC (National Fellowship for Women in Science, México). MMA and GTdS acknowledge funding provided by CONAHCyT in the form of Scholarships as members of the National System of Researchers (grant SNI 26048 and SNI 256730). This research was partially funded by Tecnologico de Monterrey. We also acknowledge the primary antibodies provided by Santa Cruz Biotechnology Inc. in the form of free samples. SOMC and MR acknowledge the support of Federico Baur Endowed Chair in Nanotechnology (ILST002-23ID69001). SOMC and MR also acknowledge the support of provided by CONAHCyT in the form of scholarships as members of the National System of Researchers(grant SNI 31803 and SNI 1047863).

References

1 J. Kim, C. M. Hope, N. Gantumur, G. B. Perkins, S. O. Stead, Z. Yue, X. Liu, A. U. Asua, F. D. Kette, D. Penko,

C. J. Drogemuller, R. P. Carroll, S. C. Barry, G. G. Wallace and P. T. Coates, *Adv. Funct. Mater.*, 2020, **30**, 2000544.
2 J. P. Quint, M. Samandari, L. Abbasi, E. Mollocana, C. Rinoldi, A. Mostafavi and A. Tamayol, *Nanoscale*, 2022, **14**, 797–814.
3 Q. Feng, D. Li, Q. Li, X. Cao and H. Dong, *Bioact. Mater.*, 2022, **9**, 105–119.
4 C. Cha, J. Oh, K. Kim, Y. Qiu, M. Joh, S. R. Shin, X. Wang, G. Camci-Unal, K. Wan, R. Liao and A. Khademhosseini, *Biomacromolecules*, 2014, **15**, 283–290.
5 R.-S. Hsu, P.-Y. Chen, J.-H. Fang, Y.-Y. Chen, C.-W. Chang, Y.-J. Lu and S.-H. Hu, *Adv. Sci.*, 2019, **6**, 1900520.
6 X. Zhao, S. Liu, L. Yildirimer, H. Zhao, R. Ding, H. Wang, W. Cui and D. Weitz, *Adv. Funct. Mater.*, 2016, **26**, 2809–2819.
7 Y. Fang, Y. Guo, M. Ji, B. Li, Y. Guo, J. Zhu, T. Zhang and Z. Xiong, *Adv. Funct. Mater.*, 2022, **32**, 2109810.
8 K. Liu, Z. Zhu, X. Wang, D. Gonçalves, B. Zhang, A. Hierlemann and P. Hunziker, *Nanoscale*, 2015, **7**, 16983–16993.
9 S. R. Shin, C. Zihlmann, M. Akbari, P. Assawes, L. Cheung, K. Zhang, V. Manoharan, Y. S. Zhang, M. Yüksekkaya, K. Wan, M. Nikkhah, M. R. Dokmeci, X. S. Tang and A. Khademhosseini, *Small*, 2016, **12**, 3677–3689.
10 D. Y. Santiesteban, K. Kubelick, K. S. Dhada, D. Dumani, L. Suggs and S. Emelianov, *Ann. Biomed. Eng.*, 2016, **44**, 750–772.
11 X. Zhou, F. Chen, H. Lu, L. Kong, S. Zhang, W. Zhang, J. Nie, B. Du and X. Wang, *Ind. Eng. Chem. Res.*, 2019, **58**, 10922–10930.
12 A. Pepe, P. Podesva and G. Simone, *Sci. Rep.*, 2017, **7**, 6014.
13 F. Nasrollahi, F. Nazir, M. Tavafoghi, V. Hosseini, M. A. Darabi, D. Paramelle, A. Khademhosseini and S. Ahadian, *Adv. NanoBiomed Res.*, 2021, **1**, 2000113.
14 Q. Cheng, A. Hao and P. Xing, *Adv. Colloid Interface Sci.*, 2020, **286**, 102301.
15 S. Nikazar, V. S. Sivasankarapillai, A. Rahdar, S. Gasmi, P. S. Anumol and M. S. Shanavas, *Biophys. Rev.*, 2020, **12**, 703–718.
16 M. K. Kumawat, M. Thakur, R. B. Gurung and R. Srivastava, *Sci. Rep.*, 2017, **7**, 15858.
17 B. Geng, F. Fang, P. Li, S. Xu, D. Pan, Y. Zhang and L. Shen, *Chem. Eng. J.*, 2021, **417**, 128125.
18 M. Frieler, C. Pho, B. H. Lee, H. Dobrovolny, G. R. Akkaraju and A. V. Naumov, *Nanomaterials*, 2021, **11**, 140.
19 H. Bian, Q. Wang, S. Yang, C. Yan, H. Wang, L. Liang, Z. Jin, G. Wang and S. F. Liu, *J. Mater. Chem. A*, 2019, **7**, 5740–5747.
20 D. Qu, M. Zheng, L. Zhang, H. Zhao, Z. Xie, X. Jing, R. E. Haddad, H. Fan and Z. Sun, *Sci. Rep.*, 2014, **4**, 5294.
21 L. L. Zhang, X. Zhao, H. Ji, M. D. Stoller, L. Lai, S. Murali, S. Mcdonnell, B. Cleveger, R. M. Wallace and R. S. Ruoff, *Energy Environ. Sci.*, 2012, **5**, 9618–9625.
22 M. Miah, S. Bhattacharya, A. Gupta and S. K. Saha, *Electrochim. Acta*, 2016, **222**, 709–716.
23 A. P. Alivisatos, W. Gu and C. Larabell, *Annu. Rev. Biomed. Eng.*, 2005, **7**, 55–76.
24 H. Wang, C. Qi, A. Yang, X. Wang and J. Xu, *Nanomaterials*, 2021, **11**, 2798.
25 Y. Pang, H. Gao, L. Lai and X. Li, *Mater. Res. Bull.*, 2018, **104**, 83–86.
26 A. B. Siddique, K. Morrison, G. Venkat, A. K. Pramanick, N. Banerjee and M. Ray, *ACS Appl. Electron. Mater.*, 2021, **3**, 1437–1446.
27 N. Motohashi and A. Asakura, *Front. Cell Dev. Biol.*, 2014, **2**, 78853.
28 E. J. Bolívar-Monsalve, C. F. Ceballos-González, K. I. Borrayo-Montaño, D. A. Quevedo-Moreno, J. F. Yee-de León, A. Khademhosseini, P. S. Weiss, M. M. Alvarez and G. Trujillo-de Santiago, *Bioprinting*, 2021, **21**, e00125.
29 S. Ostrovidov, S. Salehi, M. Costantini, K. Suthiwanich, M. Ebrahimi, R. B. Sadeghian, T. Fujie, X. Shi, S. Cannata, C. Gargioli, A. Tamayol, M. R. Dokmeci, G. Orive, W. Swieszkowski and A. Khademhosseini, *Small*, 2019, **15**, 1805530.
30 J. H. Kim, Y.-J. Seol, I. K. Ko, H.-W. Kang, Y. K. Lee, J. J. Yoo, A. Atala and S. J. Lee, *Sci. Rep.*, 2018, **8**, 12307.
31 T. P. T. Nguyen, F. Li, S. Shrestha, R. S. Tuan, H. Thissen, J. S. Forsythe and J. E. Frith, *Biomaterials*, 2021, **279**, 121214.
32 H. Wang, H. Liu, H. Liu, W. Su, W. Chen and J. Qin, *Adv. Mater. Technol.*, 2019, **4**, 1800632.
33 J. M. Lee, J. W. Choi, C. D. Ahrberg, H. W. Choi, J. H. Ha, S. G. Mun, S. J. Mo and B. G. Chung, *Microsyst. Nanoeng.*, 2020, **6**, 1–10.
34 E. J. Bolívar-Monsalve, C. F. Ceballos-González, C. Chávez-Madero, B. G. de la Cruz-Rivas, S. Velásquez-Marín, S. Mora-Godínez, L. M. Reyes-Cortés, A. Khademhosseini, P. S. Weiss, M. Samandari, A. Tamayol, M. M. Alvarez and G. Trujillo-de Santiago, *Adv. Healthcare Mater.*, 2022, **11**(24), 2200448.
35 M. H. Gass, U. Bangert, A. L. Bleloch, P. Wang, R. R. Nair and A. K. Geim, *Nat. Nanotechnol.*, 2008, **3**, 676–681.
36 L. Tang, R. Ji, X. Li, K. S. Teng and S. P. Lau, *J. Mater. Chem. C*, 2013, **1**, 4908–4915.
37 Q. Yang, J. Duan, W. Yang, X. Li, J. Mo, P. Yang and Q. Tang, *Appl. Surf. Sci.*, 2018, **434**, 1079–1085.
38 M. T. Hasan, R. Gonzalez-Rodriguez, C. Ryan, N. Faerber, J. L. Coffer and A. V. Naumov, *Adv. Funct. Mater.*, 2018, **28**, 1804337.
39 V. Țucureanu, A. Matei and A. M. Avram, *Crit. Rev. Anal. Chem.*, 2016, **46**, 502–520.
40 S. Liu, J. Tian, L. Wang, Y. Zhang, X. Qin, Y. Luo, A. M. Asiri, A. O. Al-Youbi and X. Sun, *Adv. Mater.*, 2012, **24**, 2037–2041.
41 Y. Yang, J. Cui, M. Zheng, C. Hu, S. Tan, Y. Xiao, Q. Yang and Y. Liu, *Chem. Commun.*, 2011, **48**, 380–382.
42 L. Tang, R. Ji, X. Cao, J. Lin, H. Jiang, X. Li, K. S. Teng, C. M. Luk, S. Zeng, J. Hao and S. P. Lau, *ACS Nano*, 2012, **6**, 5102–5110.

43 K. Gómez-Lizárraga, I. Garduño-Wilches, J. Narro-Ríos, C. Piña-Barba, M. Aguilar-Frutis and G. Alarcón-Flores, *J. Nanopart. Res.*, 2022, **24**, 66.
44 D. Kurniawan and W.-H. Chiang, *Carbon*, 2020, **167**, 675–684.
45 A. B. Siddique, S. M. Hossain, A. K. Pramanick and M. Ray, *Nanoscale*, 2021, **13**, 16662–16671.
46 W. Liu, M. A. Heinrich, Y. Zhou, A. Akpek, N. Hu, X. Liu, X. Guan, Z. Zhong, X. Jin, A. Khademhosseini and Y. S. Zhang, *Adv. Healthc. Mater.*, 2017, **6**, 1601451.
47 M. H. Chen, L. L. Wang, J. J. Chung, Y.-H. Kim, P. Atluri and J. A. Burdick, *ACS Biomater. Sci. Eng.*, 2017, **3**, 3146–3160.
48 L. Li, Y. Huang, P. Zhao, H. Miao and T. Zhao, *Chem. Res. Chin. Univ.*, 2020, **36**, 955–961.
49 M. G. A. Mohamed, P. Ambhorkar, R. Samanipour, A. Yang, A. Ghafoor and K. Kim, *Biomicrofluidics*, 2020, **14**, 021501.
50 Q. Liu, B. Guo, Z. Rao, B. Zhang and J. R. Gong, *Nano Lett.*, 2013, **13**, 2436–2441.
51 H. Geng, J. Qiu, H. Zhu and X. Liu, *J. Mater. Sci.: Mater. Med.*, 2018, **29**, 85.
52 J. E. Pérez-Cortez, V. H. Sánchez-Rodríguez, S. Gallegos-Martínez, C. Chuck-Hernández, C. A. Rodriguez, M. M. Álvarez, G. Trujillo-de Santiago, E. Vázquez-Lepe and J. I. Martínez-López, *Micromachines*, 2023, **14**, 55.
53 K. K. Anpalagan, J. V. Karakkat, A. Truskewycz, A. A. Saedi, P. Joseph, V. Apostolopoulos, K. Nurgali, I. Cole, Z. Cai and D. T. H. Lai, *Nanomaterials*, 2020, **10**, 1575.
54 V. Bodiou, P. Moutsatsou and M. J. Post, *Front. Nutr.*, 2020, **7**, 506214.
55 J. Kim, H. Lee, E.-J. Jin, Y. Jo, B. E. Kang, D. Ryu and G. Kim, *Small*, 2022, **18**, 2106487.